Bragg diffraction and surface reflection of neutrons from perfect crystals at grazing incidence

A. Zeilinger and T. J. Beatty
Department of Physics, Massachusetts Institute of Technology, Cambridge, Massachusetts 02139
(Received 2 February 1983)

Bragg diffraction of neutrons incident at grazing angles on crystal surfaces has been studied both theoretically and experimentally. In the theoretical analysis, use of the complete fourth-order expression for the dispersion surface had to be made. The calculations have shown that significant modifications are expected in both the optical total reflection phenomena and in the characteristics of the Darwin diffraction plateau as compared to situations where only either process can occur. The most interesting consequences are (a) a change of the critical angle for total reflection, (b) a significant reduction of the height of the Darwin plateau and a modification of its intensity distribution, (c) pronounced shifts of the Bragg peak to angles above the critical angle, and (d) a significant reduction of the penetration depth of Bragg-diffracted radiation. An experimental study of Bragg diffraction at internal (022) planes of a large Si crystal with neutrons incident at grazing angles onto a polished external (211) surface has been performed. The wavelength distribution of that beam was characteristic of neutron-diffraction experimentation and hence broad by dynamical diffraction standards. The experimental result therefore shows features as expected from a sum of many individual reflectivity profiles and confirms both that the Bragg reflectivity is small for incidence below the critical angle and that a peak of that reflectivity occurs just above the critical angle. Practical application of the observed phenomena for the investigation of surface structures is discussed.

I. INTRODUCTION

In investigations of the crystal diffraction of neutrons one usually neglects surface-reflected beams because of the large angle of incidence used in conventional experiments. This is also characteristic of the conventional theory of dynamical diffraction[1-3] in which the mirror reflected waves are not included in the treatment. However, these waves become important for cases where the neutrons are incident on a crystal surface at shallow angles, most markedly if this angle of incidence is in the range characteristic of total mirror reflection. Equivalently, the interesting question arises as to whether the phenomenon of total reflection is influenced when the neutron beam also satisfies the Bragg condition for a set of crystal-lattice planes. The present paper deals with the Bragg case of grazing incidence both theoretically and experimentally.

As is well known, dynamical diffraction of neutrons is closely analogous to the diffraction of x rays and is generally less complicated because negligible absorption for neutrons is usually encountered. For x rays, the Bragg case of grazing incidence was given an early analysis in a general way by Farwig and Schürmann.[4] This was then extended by Kishino and Kohra[5] who investigated both the modifications in the deviation from the geometrical Bragg angle and the width of the plateau of the diffraction curve. Some of their results were disputed in later work by Brümmer *et al.*[6] and Härtwig[7] who used an approach based on a calculation of the excitation error first introduced by Bedinska.[8] In contrast, they found good agreement between their theoretical and experimental results and the predictions of Rustichelli,[9] who derived closed-form expressions for both of these quantities using geometrical considerations exploiting the fact that the dispersion surfaces asymptotically approach spheres in contrast to the conventional dynamical theory. Very recently, Vineyard[10] used distorted-wave Born-approximation (DWBA) calculations to predict the results of experiments where the diffraction of beams incident at angles below the critical angle of total reflection as proposed earlier by Eisenberger and Marra[11] is studied.

In Sec. II we will present our theoretical derivation of the complete expression of the dispersion surface and discuss the treatment of some characteristic cases. Boundary conditions lead then to the amplitudes of both the Bragg-diffracted and the mirror-reflected wave. Using this approach, calculated reflectivity curves for monochromatic radiation will be presented in Sec. III and discussed using

the properties of the dispersion surface. Section IV will then present the results of experiments in which a well-collimated neutron beam with a broad wavelength distribution (by dynamical diffraction standards) was incident at near grazing incidence upon the (211) planes of a perfect silicon crystal with the beam also satisfying Bragg-diffraction conditions for internal (022) planes. In Sec. V we discuss some possible extensions of the present work in particular applications to the study of surface phenomena and properties. It is particularly suggested that investigations of cases where a surface layer exists of a refractive index different from the bulk should be promising.

II. THE DISPERSION SURFACE

We start with the time-independent Schrödinger equation

$$\left[-\frac{\hbar^2}{2m}\nabla^2+V(\vec{r})\right]\psi(\vec{r})=E\psi(\vec{r})\ , \tag{1}$$

where m is the mass of the neutron, E is its vacuum kinetic energy, and $V(\vec{r})$ is the neutron-crystal interaction potential. Now using the ansatz

$$\psi_j(\vec{r})=u_j(\vec{r})e^{i\vec{K}_j\cdot\vec{r}}\ , \tag{2}$$

where $\vec{K}$ is an in-crystal wave vector and j designates a particular wave-field solution, and expanding both $u(\vec{r})$ and $V(\vec{r})$ into their Fourier components $u(\vec{G})$ and $V(\vec{G})$ in terms of the reciprocal-lattice vectors $\vec{G}$, we obtain the fundamental equations for dynamical diffraction of neutrons,[3]

$$\left[\frac{\hbar^2}{2m}(\vec{K}+\vec{G})^2-E\right]u(\vec{G})=-\sum_{\vec{G}'}V(\vec{G}-\vec{G}')u(\vec{G}')\ . \tag{3}$$

For the case where no lattice planes are oriented for Bragg diffraction to occur, only one of the equations (3) prevails, and

$$\left[\frac{\hbar^2}{2m}K^2-E\right]u(0)+V(0)u(0)=0\ . \tag{4}$$

Using the continuity of tangential components of wave vectors at the entrance face, we find that the in-crystal wave vector $\vec{K}$ is related to the vacuum wave vector $\vec{k}$ via

$$\vec{K}=\vec{k}+k\epsilon\hat{n}\ , \tag{5}$$

where $\hat{n}$ is a unit vector oriented normal to the surface pointing into the crystal (Fig. 1). In order to determine the excitation error ϵ and hence $\vec{K}$ from Eq. (4), we use

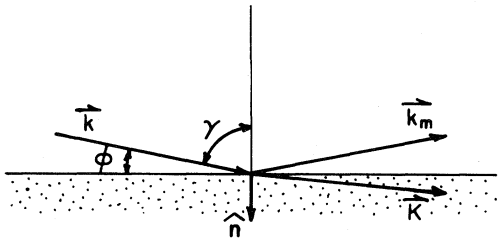

FIG. 1. Geometry in real space in the absence of Bragg diffraction (one-beam case).

$$K^2=k^2(1+2\epsilon\cos\gamma+\epsilon^2) \tag{6}$$

since $\hat{n}\cdot\vec{k}=k\cos\gamma$ (see Fig. 1). Inserting Eq. (6) into Eq. (4) gives a second-order polynomial equation for ϵ, which finally results in the following possible in-crystal wave vectors:

$$\vec{K}=\vec{k}+k\cos\gamma\left[\pm\left[1-\frac{V(0)}{E\cos^2\gamma}\right]^{1/2}-1\right]\hat{n}\ . \tag{7}$$

Here γ is the angle between the incident vacuum wave vector $\vec{k}$ and the surface normal $\hat{n}$. For shallow angles of incidence, $\cos\gamma$ varies strongly with that angle and therefore our definition of the excitation error ϵ includes $\cos\gamma$ in contrast to the conventional treatment of dynamical diffraction.[3] Equation (4) defines the dispersion surface in the one-beam case. The two possible values of $\vec{K}$ inside the crystal correspond here to a refracted wave and to that wave reflected at a possible back face of the medium. From Eq. (7) we readily obtain total reflection if the square-root term becomes imaginary.

Turning now to a case where one set of lattice planes is oriented such that Bragg diffraction may occur, the system of Eqs. (3) reduces to the two coupled equations

$$\left[\frac{\hbar^2}{2m}K^2-E+V(0)\right]u(0)+V(-\vec{G})u(\vec{G})=0\ , \tag{8a}$$

$$V(\vec{G})u(0)+\left[\frac{\hbar^2}{2m}(K+G)^2-E+V(0)\right]u(\vec{G})=0\ . \tag{8b}$$

The in-crystal wave vectors $\vec{K}$ are again related to the vacuum wave vector $\vec{k}$ through Eq. (5). In addition, we need the relation

$$(\vec{K}+\vec{G})^2=k^2\left[1+\alpha+2\epsilon\left[\cos\gamma-\frac{G}{k}\cos\beta\right]+\epsilon^2\right], \quad (9)$$

where

$$\alpha\equiv(G^2+2\vec{k}\cdot\vec{G})/k^2 \quad (10)$$

and β is the angle between crystal surface and lattice planes (Fig. 2).

In order for Eqs. (8) to have nontrivial solutions for the amplitudes u, the secular determinant of that system of equations has to vanish, which together with Eqs. (6) and (9) leads to the fourth-order polynomial equation for ϵ,

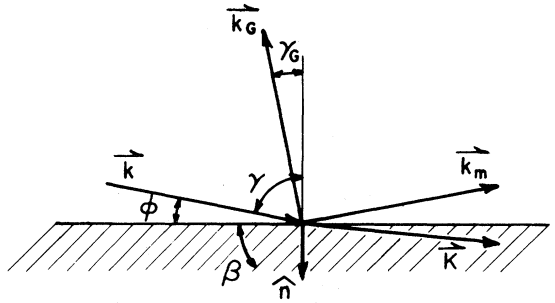

FIG. 2. Geometry in real space with asymmetric Bragg diffraction (two-beam case). The orientation of the diffracting lattice planes is indicated schematically.

$$\epsilon^4+2\left[2\cos\gamma-\frac{G}{k}\cos\beta\right]\epsilon^3+\left[\alpha+2\frac{V(0)}{E}+4\left[\cos^2\gamma-\frac{G}{k}\cos\gamma\cos\beta\right]\right]\epsilon^2$$
$$+2\left[\alpha\cos\gamma+\frac{V(0)}{E}\left[2\cos\gamma-\frac{G}{k}\cos\beta\right]\right]\epsilon+\alpha\frac{V(0)}{E}+\frac{V(0)^2}{E^2}-\frac{V(\vec{G})V(-\vec{G})}{E^2}=0\,. \quad (11)$$

This equation defines the complete dispersion surface for the two-beam case. In the conventional approach one deals only with the hyperbolic part of the surface in the vicinity of the Laue point L, which implies that quadratic terms in ϵ are neglected in Eqs. (6) and (9) thereby leading to only a second-order polynomial equation for ϵ in Eq. (11). In order to arrive at explicit results from Eq. (11), we have solved this equation numerically. During this solution procedure, special precaution must be taken to avoid numerical errors which may arise from the fact that the various values for ϵ can differ by many orders of magnitude. The number of real solutions for ϵ and hence the number of wave fields with real wave vectors inside the crystal depends strongly on the magnitude of the coefficients of Eq. (11) and hence on the geometrical parameters for the situation which is being considered.

We will now consider explicitly how the wave fields, which are excited inside the crystal, are related to the shape of the dispersion surface as obtained from Eq. (11). We shall concentrate on the case where the orientation of the crystal surface will always correspond to that of extremely asymmetric diffraction.

We first consider the case of neutrons with a vacuum wavelength large enough that the neutrons are Bragg diffracted at incident angles significantly larger than the critical angle for total reflection. This implies that the regions of total surface reflection and Bragg diffraction are well separated. Figure 3 shows the dispersion surface for that case. We start [Fig. 3(a)] with the specific case of a wave vector $\vec{k}$ which is incident at an angle above the regions of both Bragg diffraction and total reflection. As expected, four wave fields as signified by the four tie points A_1 to A_4 are excited inside the crystal. In the conventional dynamical diffraction analysis of the Bragg case only the tie points A_2 and A_3 are considered for the case of a plane parallel crystal plate. The wave fields associated with A_1 and A_4 are not found in that approach since there the asymptotes to the hyperbolic part of the dispersion surface are not taken as spheres. Also indicated are the directions of the neutron probability density currents $\vec{j}$—the analog to the energy density current in x-ray diffraction. These directions are oriented normal to the dispersion surface at the tie points. We find that the neutron currents for the two wave fields associated with A_3 and A_4 are pointing towards the crystal surface. These wave fields would arise from reflection at the back face of the crystal and hence we may neglect these wave fields for a semi-infinite crystal as considered here. Only the wave fields associated with A_1 and A_2 are propagating into the crystal. Of these, wave field 1 arises from back reflection of the Bragg-diffracted wave into the crystal at the entrance face. In a quantitative analysis it was found that this wave is of very small amplitude. Thus only wave field 2 is of significant amplitude inside the semi-infinite crystal.

If we now consider rotating the incident wave vector to shallower angles of incidence, we arrive at a situation where the surface normal through the tail of $\vec{k}$ passes through the gap between the two branches of the dispersion surface [Fig. 3(b)]. Therefore only two real solutions for ϵ are obtained, the other two being complex conjugates leading to

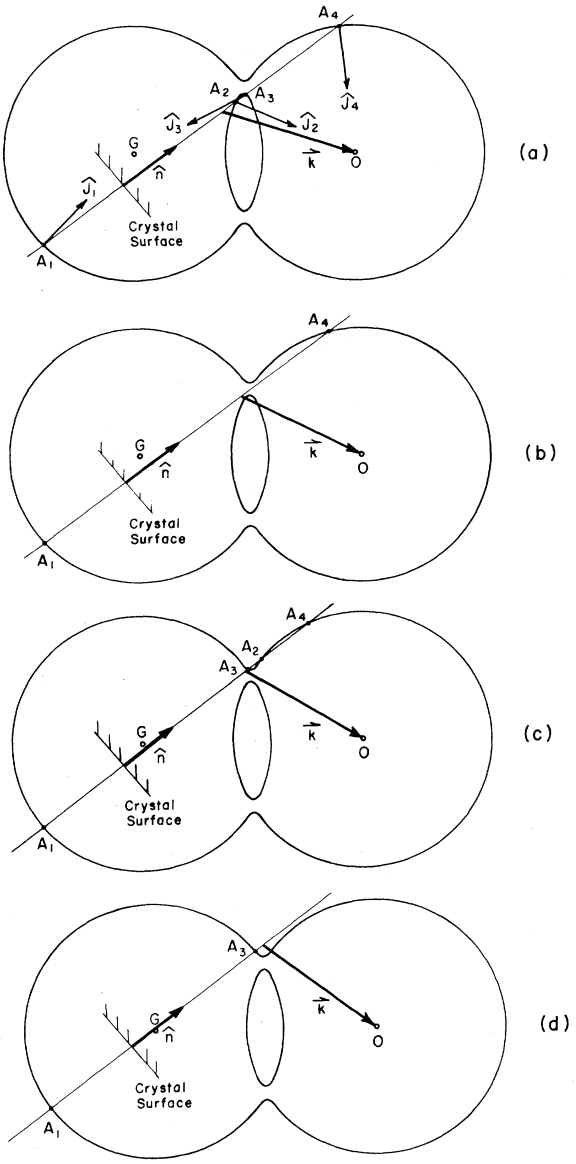

FIG. 3. Geometry in reciprocal space for asymmetric Bragg diffraction near "grazing" incidence showing the dispersion surface. From (a) to (d) the angle of incidence of the vacuum wave vector $\vec{k}$ with respect to the crystal surface is systematically lowered. Four distinctly different regions of diffraction are observed (see text).

two complex solutions for $\vec{K}$. Of these, only the one which gives an exponentially decaying wave field is physical for a semi-infinite crystal. This is also known as the Darwin plateau region where only negligibly small intensity may propagate deep into the crystal since the amplitude associated with A_1 is still found to be very small.

Reducing the angle of incidence further [Fig. 3(c)] leads then to a situation where we have again four real tie points, but now they are arranged on the same branch of the dispersion surface. Here again, propagation of intensity into the crystal may occur and it is again the wave fields associated with the tie points A_1 and A_2 which are physical for the case of a semi-infinite crystal and of them only A_2 is of significant amplitude.

An even further reduction of the angle of incidence leads to the two tie points A_2 and A_4 moving close together until they coalesce in one point. This point gives the critical angle for total reflection since at smaller angles of incidence we are left again with only two real tie points A_1 and A_3 [Fig. 3(d)], of these only A_1 is physical, but again with negligible amplitude, for the semi-infinite crystal.

Thus for that specific choice of wavelength and surface orientation four well-distinguishable regions exist which are characterized by the number and type of real tie points excited. We now wish to point out that situations exist where for grazing incidence such is not the case. To analyze that possibility we imagine an experiment where the incident neutrons would fulfill the Bragg condition at shallower angles of incidence, this implies shorter wavelength neutrons if we keep the orientation of the reflecting lattice planes with respect to the surface unchanged. Therefore, the dispersion surface will be larger with respect to $\vec{G}$ as shown in Fig. 4.

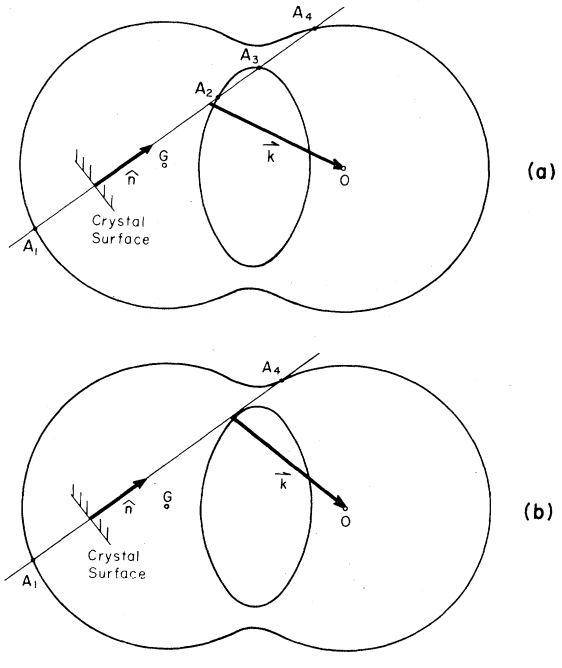

FIG. 4. Dispersion surface for a more asymmetric case than Fig. 3. Here only two different regions are observed when the angle of incidence is lowered. This case occurs at shorter wavelengths as compared to Fig. 3.

We again consider first an angle of incidence which is oriented in a direction much larger than both the Bragg-diffraction and total-reflection regions [Fig. 4(a)]. Here we excite four real tie points in a completely analogous way to Fig. 3(a) above. If we now decrease the angle of incidence we enter again the region where only two real tie points are excited. The interesting difference to the situation discussed above is that a further reduction of the angle of incidence will never result in a situation such as the one shown in Fig. 3(c), where again four real tie points were excited below the Bragg-diffraction region. As can be seen from studying Fig. 4 this behavior is due to the property, that in the region around the Laue point the curvature of the dispersion surface is significantly different from that of the asymptotic spheres. As we will see in the next section when we calculate the amplitudes of the mirror-reflected and Bragg-diffracted waves, this behavior implies that total reflection is considerably changed by Bragg diffraction in that region and that the angular regions of total reflection and of Bragg diffraction are not well separated.

III. THE REFLECTIVITY PROFILES

We now set out to calculate both the mirror and the Bragg reflectivity as a function of the angle of incidence. Therefore, we have to establish the vacuum and the in-crystal wave fields and use matching boundary conditions. Again, we restrict our considerations to the semi-infinite crystal.

The wave function outside the crystal may be written as

$$\psi_{\text{vac}}=u_0 e^{i\vec{k}\cdot\vec{r}}+u_G e^{i\vec{k}_G\cdot\vec{r}}+u_m e^{i\vec{k}_m\cdot\vec{r}}, \tag{12}$$

where u_0, u_G, and u_m are the amplitudes of the incident, Bragg-diffracted, and mirror-reflected waves, respectively. The wave vector of the Bragg-diffracted wave $\vec{k}_G$ may differ from $\vec{k}+\vec{G}$ only by a vector normal to the surface, hence

$$\vec{k}_G=\vec{k}+\vec{G}+k\,\delta\vec{n} \tag{13}$$

where δ may be defined by setting k_G^2 equal to k^2 because of energy conservation. The wave vector $\vec{k}_m$ of the mirror-reflected wave is related to the incident wave vector $\vec{k}$ through (Fig. 2)

$$\vec{k}_m=\vec{k}-2k\cos\gamma\hat{n} \tag{14}$$

since it has the same tangential component as $\vec{k}$, but opposite normal component.

As we found in the preceding section, inside the semi-infinite crystal we have to consider only two wave fields, 1 and 2, with each of them being a superposition of a forward (0) and a Bragg-diffracted ($\vec{G}$) wave,

$$\psi_{\text{cryst}}=u_1(0)e^{i\vec{K}_1\cdot\vec{r}}+u_1(\vec{G})e^{i(\vec{K}_1+\vec{G})\cdot\vec{r}}+u_2(0)e^{i\vec{K}_2\cdot\vec{r}}+u_2(\vec{G})e^{i(\vec{K}_2+\vec{G})\cdot\vec{r}}. \tag{15}$$

Here the in-crystal wave vectors $\vec{K}$ are given as solutions to Eq. (11) together with Eq. (5). Boundary conditions now require that both the wave function and its derivative are continuous at the surface, so that there,

$$\psi_{\text{vac}}=\psi_{\text{cryst}} \tag{16a}$$

and

$$\frac{\partial}{\partial(\hat{n}\cdot\vec{r})}\psi_{\text{vac}}=\frac{\partial}{\partial(\hat{n}\cdot\vec{r})}\psi_{\text{cryst}}\,. \tag{16b}$$

These conditions, together with Eqs. (8), completely determine the amplitudes. We note that if we had omitted the very weakly excited wave field 1, thus reducing the number of unknown amplitudes, we would arrive at an overdetermined system of equations.

We have performed detailed numerical calculations of the reflectivities as a function of the angle of incidence for various wavelengths. These wavelengths were chosen such that they fulfill the geometrical Bragg condition, i.e., the Bragg condition when refraction is neglected, for shallow to grazing angles of incidence. The specific situation chosen was that of the experiment, where Bragg diffraction was studied at internal (022) planes of a Si crystal with the crystal surface being parallel to the (211) planes. Table I lists the parameters significant for the calculations. With these parameters held fixed, the reflectivity profile of intensity versus the angle of incidence was calculated for different selected wavelengths as shown in Figs. 5–8. There the geometrical Bragg condition for each reflectivity profile was satisfied at a specific angle with respect to the surface.

In Fig. 5 the wavelength was chosen such that it would fulfill the geometrical Bragg condition at an incidence angle 2′ above the surface. The bottom part of the figure displays the Bragg reflectivity profile which has a shape still rather similar to the usu-

TABLE I. Interplanar spacing d, Fourier coefficients of the crystal potential V, and angle β betwen the (022) planes and the crystal surface used in the calculations.

$d(022)$	1.920 Å
$V(0)$	5.40×10^{-8} eV
$V(022)$	5.24×10^{-8} eV
β	54.74°

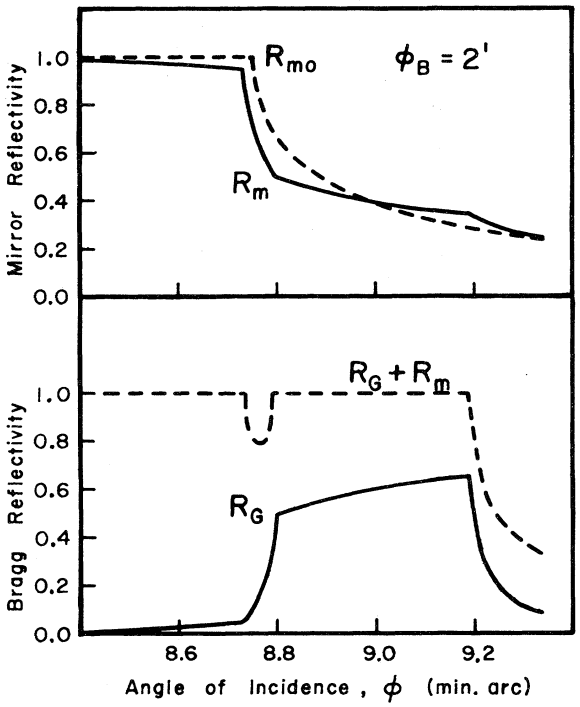

FIG. 5. Reflectivities for neutrons of wavelength $\lambda = 3.1369$ Å as a function of the angle of incidence with respect to the (211) surfaces of a Si crystal. Neutrons of that wavelength would fulfill the geometrical Bragg condition for diffraction at the internal (022) planes at an angle $\phi_B = 2'$ above the surface. The top of the figure compares the mirror reflectivity R_m predicted for the case of simultaneous Bragg diffraction with the mirror reflectivity R_{mo} in the absence of Bragg diffraction. R_G is the reflectivity of the Bragg beam.

al Darwin plateau. The essential modifications are that the Bragg reflectivity does not reach 100% and that its plateau height is not constant. This is to be understood because the radiation is also diverted by the competing process of surface mirror reflection. The top part of Fig. 5 shows the mirror reflectivity curve together with that expected for an amorphous specimen where no competing Bragg-diffraction process is present. Here we notice that within the range of angles plotted this reflectivity likewise does not reach 100% even below the critical angle. The reflectivity for angles below the center of the modified Darwin plateau is always below that of the amorphous medium while above that region the reflectivity is found to be higher. This may be understood from the fact that at low angles we excite α-branch radiation inside the crystal which has its antinodes at the lattice planes and thus experiences a lower effective potential. The β-branch radiation excited at higher angles experiences a higher potential because it has its nodes at the crystal-lattice planes. Thus the mirror reflectivity at higher angles is larger than that of the amorphous specimen. Although neither the mirror-reflected nor the Bragg-diffracted beams achieve 100% reflectivity, it is interesting that their sum does that very well. In Fig. 5, we also show that a sum of unity is found both within the modified Darwin plateau and mirror total reflection ranges as required by the property that in these regions only exponentially attenuated wave fields may have sizable amplitude inside the crystal. Both ranges mentioned above are well separated as indicated by the dip in the sum reflectivity profile. Thus at this and at longer wavelengths all four regions as presented in Fig. 3 are observed.

Figure 6 shows the results for a slightly shorter wavelength beam such that the geometrical Bragg condition would be fulfilled at 1′ above the surface. Here a low-angle edge of the Darwin curve can no longer be identified. Also, there exists no dip in the curve representing the sum of mirror and Bragg reflectivity. Its 100% range extends all the way out to the high-angle edge of the modified Darwin curve. This is the case as shown in Fig. 4 where the surface normal can only cut the dispersion surface at four real points for angles of incidence above the Bragg region and not below. Also, here the shape of the mirror reflectivity curve is strongly modified as

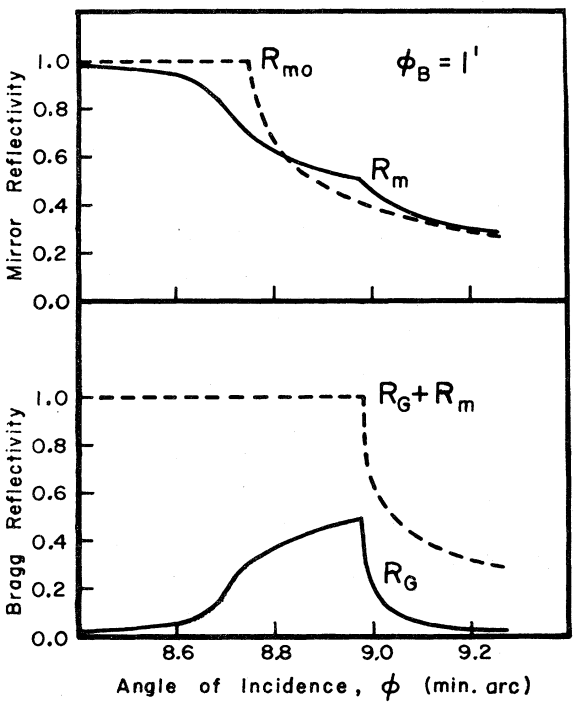

FIG. 6. As in Fig. 5, but for $\lambda = 3.1362$ Å, i.e., $\phi_B = 1'$.

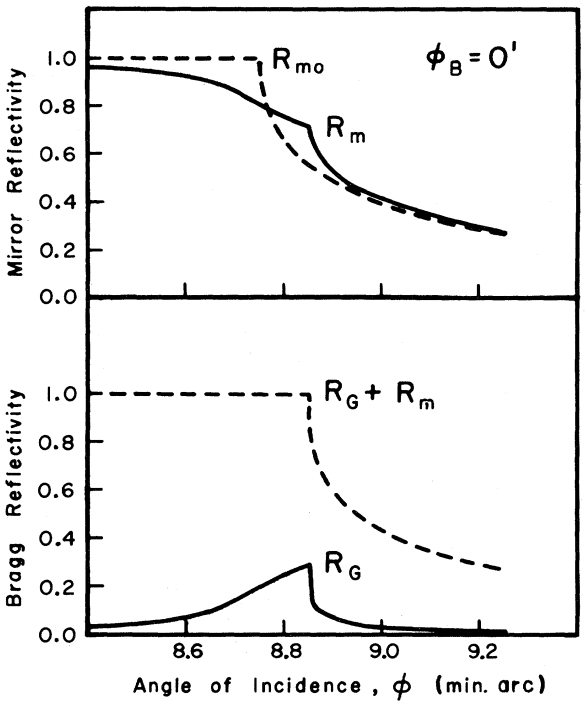

FIG. 7. As in Fig. 5, but for $\lambda = 3.1356$ Å, i.e., $\phi_B = 0'$.

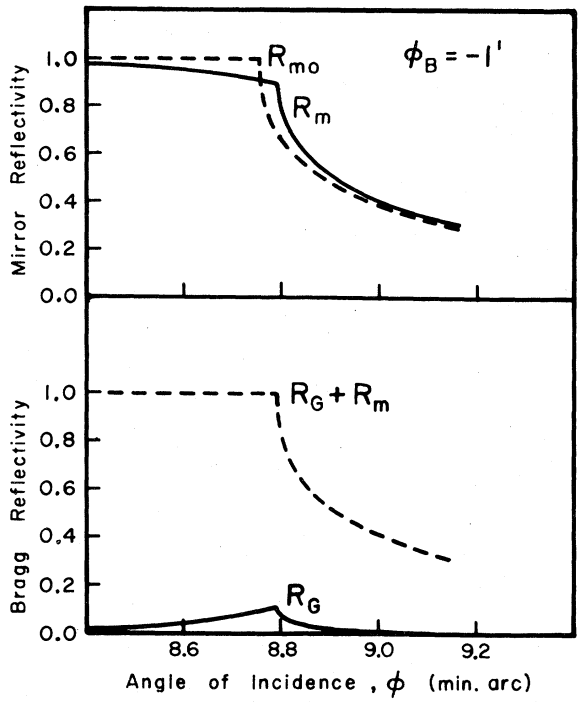

FIG. 8. As in Fig. 5, but for $\lambda = 3.1349$ Å, i.e., $\phi_B = -1'$.

compared to the reflectivity of the amorphous specimen. These features are essentially retained at shorter wavelengths. Figures 7 and 8 show the reflectivities for neutrons fulfilling the geometrical Bragg condition at exactly grazing incidence or even at *negative* angles of incidence. An interesting property of these latter cases is that the kink in the mirror reflectivity due to the high-angle limit of the modified Darwin plateau has now moved so close to the critical angle for the amorphous specimen that it appears as if that critical angle were shifted up to higher angles of incidence. For all of these curves, the peak of the Bragg reflectivity occurs at angles above the total reflection critical angle, although some reflectivity may still be observed at smaller angles due to the shape of the modified Darwin curves similar to the x-ray case.

In all of these cases the angular position of the Bragg peak is strongly shifted with respect to the geometrical Bragg law because of pronounced refraction at the entrance surface. Conventional dynamical diffraction theory[1] predicts for this shift

$$\delta\theta_B = \frac{V(0)/E}{2\sin(2\theta_B)}\left[1+\frac{\cos\gamma_G}{\sin\phi_B}\right], \tag{17}$$

where θ_B is the geometrical Bragg angle and ϕ_B is the angle of the geometrical Bragg position above the surface. The conventional theory also predicts the width of the total reflection region to be

$$w = \frac{2V(\vec{G})/E}{\sin(2\theta_B)}\left[\frac{\cos\gamma_G}{\sin\phi_B}\right]^{1/2}. \tag{18}$$

Rusticchelli[9] has pointed out that these relations must break down for grazing angles of incidence because the conventional theory assumes the asymptotes to the hyperbolic parts of the dispersion surface to be straight lines. Using circles as the asymptotes, he obtains from purely geometrical considerations

$$\delta\theta_B = \left\{-\sin\phi_B + \left[\sin^2\phi_B + \frac{\sin\phi_B}{\sin(2\theta_B)}\frac{V(0)}{E}\left[1+\frac{\cos\gamma_G}{\sin\phi_B}\right]\cos\phi_B\right]^{1/2}\right\} \Big/ \cos\phi_B \tag{19}$$

for the deviation from the geometrical Bragg law and

$$w = \sin\phi_B\left[\sin^2\phi_B + \frac{\sin\phi_B}{\sin(2\theta_B)}\frac{V(0)}{E}\left[1+\frac{\cos\gamma_G}{\sin\phi_B}\right]\cos\phi_B\right]^{-1/2}\frac{2V(\vec{G})/E}{\sin(2\theta_B)}\left[\frac{\cos\gamma_G}{\sin\phi_B}\right]^{1/2} \tag{20}$$

for the width of the Darwin plateau. We have compared these expressions with the results obtained from our dynamical theory calculations for the case defined above, i.e., a fixed angle between reflecting lattice planes and crystal surface. Thus the wavelength had to be varied for obtaining values of w and $\delta\theta_B$ as a function of ϕ_B.

Figure 9 shows the deviation from the geometrical Bragg law as determined from the center position of our numerically generated modified Darwin curves together with both that of the conventional expression and of the Rusticchelli formulation. It is evident that the agreement with the latter is excellent. We need to explain how the center of the Darwin plateau was obtained for those curves where the low-angle edge of the plateau is not defined as is the case in Figs. 6–8. For such cases we selected the center to be that position where the modified mirror reflectivity agrees with that of the amorphous specimen as indicated in the top part of these figures. This is a sensible definition since at that position the surface normal passes through the Lorentz point, the center point of the hyperbolic part of the dispersion surface. We remark that for all of the curves where the lower angle edge of the Darwin plateau is clearly defined, its center position coincided with the point as defined above. Thus it appears that Rusticchelli's expression is valid even for wavelengths where the geometrical Bragg condition is satisfied at incidence angles below the surfaces (negative ϕ_B).

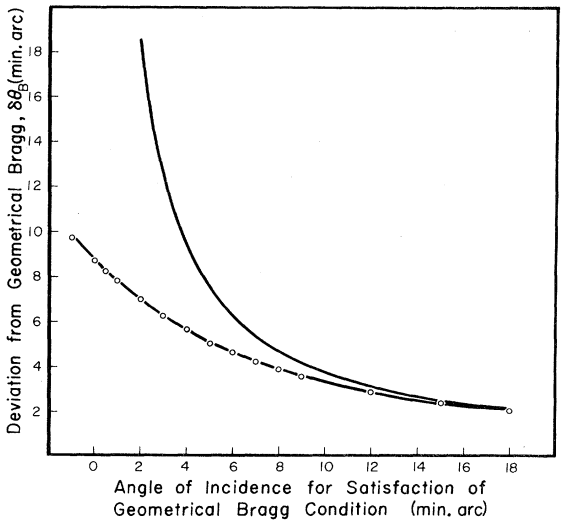

FIG. 9. Deviation from the geometrical Bragg law for diffraction at internal (022) planes as a function of the angle of incidence with respect to the (211) surface. Our numerical results (○) obtained by using the complete expression for the dispersion surface are compared both with Rusticchelli's equation (bottom curve) and with the prediction of the conventional dynamical theory.

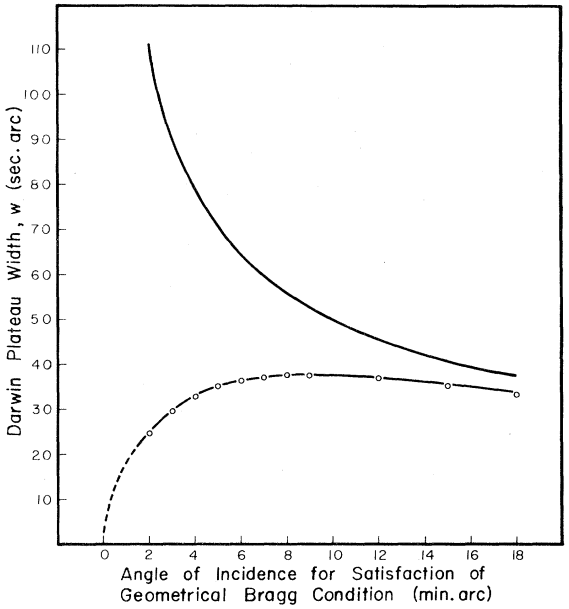

FIG. 10. Comparison of our numerical results for the Darwin plateau width (○) with Rusticchelli's equation (bottom curve) and the prediction of the conventional dynamical theory.

Figure 10 shows the width of the Darwin plateau as obtained from our numerical calculation together again with the prediction from conventional theory and from Rusticchelli's modified equation. Again excellent agreement with the latter is observed for the points shown. Here we did not include any points at low incidence angles where the low-angle edge and hence the width of the Darwin plateau are not defined anymore. One indication that Rusticchelli's expression has to break down for very small angles is seen from the property that he predicts $w=0$ for $\phi_B=0$, which obviously is not true if we refer to Fig. 7 which pictures just that case and shows a finite angular width Bragg reflectivity. This breakdown of Rusticchelli's approach is due to the fact that at these small angles the modification of the hyperbolic part of the dispersion surface by the fact that its asymptote is a sphere has to be considered. He considered the dispersion surface to be hyperbolic at its center and to be a sphere far away with no analysis of the intermediate behavior. An important point to be emphasized is, that at low angles of incidence, the width of the Darwin plateau is not proportional to the integrated reflectivity as is the case at high angles of incidence. This arises because the height of the Darwin plateau differs from unity at low angles of incidence. In fact, it varies with the angle of incidence and this is indicative of

the competing process of mirror reflection.

Another significant quantity is the penetration depth of the neutrons into the crystal. This penetration depth is finite for those angles of incidence where the sum of the mirror and the Bragg reflectivities equals unity and it is quantitatively related to the imaginary part ϵ_i of the excitation error [Eq. (5)] via

$$t=\frac{1}{k\epsilon_i} . \tag{21}$$

Here t is defined as that depth measured in a direction normal to the surface where the amplitude of the neutron wave field has decreased to $1/e$ of its value at the surface. Figure 11 exhibits that penetration depth for $\lambda=3.1369$ Å neutrons as a function of the angle of incidence both with and without internal Bragg diffraction. An interesting feature is that the minimum penetration depth within the Darwin plateau is found to be only $t=0.36$ μm which has to be compared with $t=15.6$ μm which is found for symmetric Bragg diffraction of that same wavelength.

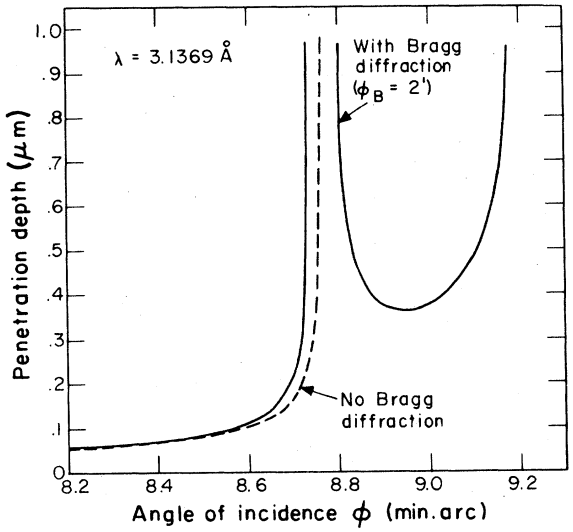

FIG. 11. Calculated penetration depth for $\lambda=3.1369$ Å neutrons both without and with Bragg diffraction at internal (022) planes ($\phi_B=2'$).

IV. EXPERIMENTAL STUDY

In the experiment, Bragg-case diffraction at internal (022) planes in a perfect Si crystal was studied with neutrons incident at grazing angles onto the crystal surface. The crystal was a cylindrical ingot of length 205 mm and about 54 mm diameter with axial direction parallel to the [111] crystallographic direction. One side of the ingot was cut to form a long flat surface of area 25×205 mm^2 parallel to the (211) planes. This implies that a set of diffracting (022) planes was oriented at an angle of 54.74° with respect to that surface. This surface was used as the mirror reflecting surface and it was necessary to be of mirror quality. This was achieved by first polishing and lapping the crystal surface with diamond grit down to 1 μm size and finally using a chemical syton polish. The flatness of the surface was established by fringe observations with an optical flat and He light. This revealed a continuous variation of the surface depth of 0.6 μm over a distance of 20 mm on the crystal surface, which is well within the requirements of the experiment.

A schematic diagram of the spectrometer arrangement is shown in Fig. 12. Neutrons reflected from a

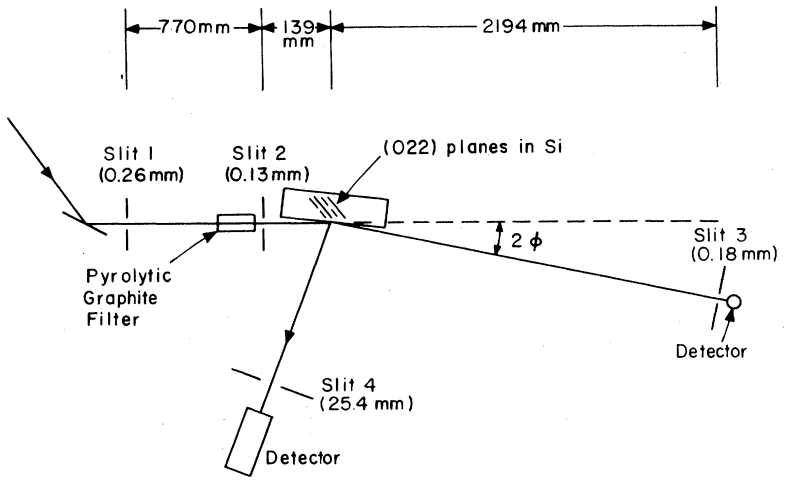

FIG. 12. Schematic diagram of the experiment studying the Bragg diffraction of neutrons at internal (022) planes in Si under the simultaneous presence of mirror reflection at the (211) surface.

graphite monochromator were passed through a slit system to form a beam of 1.16′ nominal angular width at half maximum. The primary wavelength in this beam was selected to be 3.137 Å and measurements showed it be of full width at half maximum (FWHM) of 0.029 Å. This beam was passed through an oriented pyrolitic graphite filter for attenuation of the second-order wavelength neutrons which are normally present.

Both end faces of the crystal were covered with cadmium absorber plates. This ensured that neutrons would enter and leave the crystal only through the mirror polished surface. These absorbing edges were also convenient for aligning the crystal face parallel to the beam both horizontally and vertically. Measurements of the surface-reflected beam provided then a check of the alignment of the apparatus and also gave an independent determination of the angular position of the crystal surface relative to the incident beam.

It is significant that, for very shallow angles of incidence, the Bragg-diffracted beam becomes very broad and in fact becomes significantly wider than the 25.4-mm-wide aperture slit in front of the detector. This stems from the extremely high asymmetry of the arrangement and the geometrical width W_f of the diffracted beam is given as

$$W_f = W_i \frac{\sin(2\theta_B)}{\sin\phi} , \tag{22}$$

where W_i is the geometrical width of the incident beam that had experimentally been determined to be $W_i = 210\,\mu$m FWHM.

In order to obtain the full Bragg-reflection intensity, it was thus necessary to correct the measured intensities for small angles of incidence ϕ by the formula of Eq. (22). To ascertain that the diffracted beam was actually as wide as given by Eq. (22), a series of width profiles of the Bragg beam was determined experimentally for a set of characteristic angular settings of the crystal by screening the detector with a 12.7-mm-wide slit across the diffracted beam. Figure 13 gives us an example of the intensity distribution for an angle of incidence of $\phi = 12.2'$. For that angle of incidence we expect widening of the beam by the factor 265 as is indicated by the expected beam width in Fig. 13. The measured beam widths were thus found to be in reasonable agreement with Eq. (22) which was therefore used later to adjust the experimental intensities.

Since the wavelength band used in our experiment was very broad on a dynamical diffraction scale, we could not expect to directly observe the reflectivity functions as calculated and shown in the preceding paragraph. Therefore a convolution calculation was

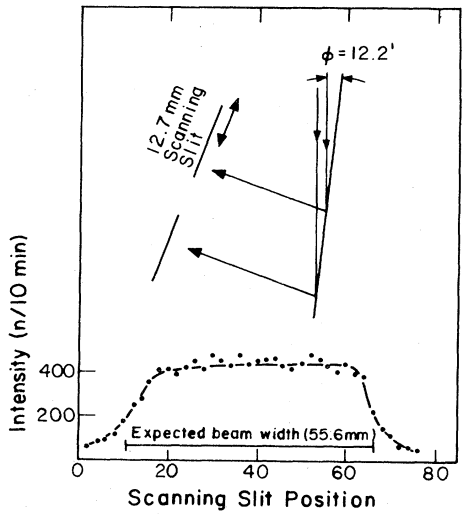

FIG. 13. A typical measurement result of the width of the beam after strongly asymmetric diffraction. The width of the incident beam was 210 μm.

performed taking into account the directional spread of neutrons in the incident beam. Figure 14 shows the result obtained for the intensity of the Bragg-diffracted beam as a function of the angular orientation of the crystal for the assumption of a very broad wavelength band. We note that only a negligibly small fraction is expected to be Bragg diffracted if the angle of incidence is below the critical angle. Furthermore, a peak is predicted just above the critical angle. This peak is of considerable interest and it stems from the property that the shift in Bragg position from Bragg's law is always such that

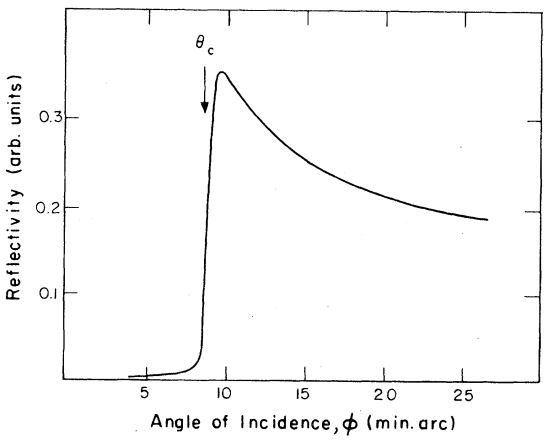

FIG. 14. Bragg reflectivity predicted for the experimental parameters taking into account both the angular spread and the wavelength distribution which was broad on a dynamical diffraction scale.

it shifts most of the Bragg-diffraction reflectivity to incidence angles just above the critical angle as may be seen from Figs. 5—8. It was also found from the calculations that the position and shape of this peak is independent of the short wavelength cutoff assumed for the calculations as long as that cutoff is at a wavelength whose geometrical Bragg position is well below the critical angle. This independence is due to the property that the Bragg reflectivity rapidly becomes very small with decreasing wavelengths (Figs. 5—8).

All of these predicted features are readily visible in the experimental result as shown in Fig. 15. We observe some intensity being reflected below the critical angle of our primary wavelength. This arises mainly from the second-order wavelength contamination of the beam and which had been found to be still 26% of the beam even with passage through the graphite filter. It is worthwhile pointing out that the falloff edge of the reflectivity of this second-order contribution occurs at just half the falloff angle of the first-order radiation corresponding to its half wavelength. It is interesting to consider the angular position of the high-angle cutoff of the measured intensity or, equivalently its width since its low-angle position is being fixed by the critical angle. This width in the experiment is about 26′, which may be compared with the prediction based on Bragg's law and our known wavelength spread. From this we would expect the width to be 44′ and this was verified experimentally by measuring the Bragg-reflection width from the same (022) lattice planes but with a beam incident on the front face of the crystal, i.e., in Bragg geometry without mirror surface reflection. It appears that this shrinking of the angular width of the measured Bragg reflectivity is related to the cutoff at the critical angle. This implies that a significant fraction of the incident beam never gets into the Bragg-diffraction region due to its short wavelength.

V. CONCLUDING COMMENTS

An interesting extension of the present experiment work will concern a detailed study of the Darwin reflectivity curves and of the modifications of the surface reflectivity in the vicinity of the critical angle as shown in Figs. 5—8. Such studies would require a beam not only collimated to at least the standards of the present experiment but also better defined on the wavelength scale, i.e., a beam monochromatized by perfect crystal diffraction as opposed to the mo-

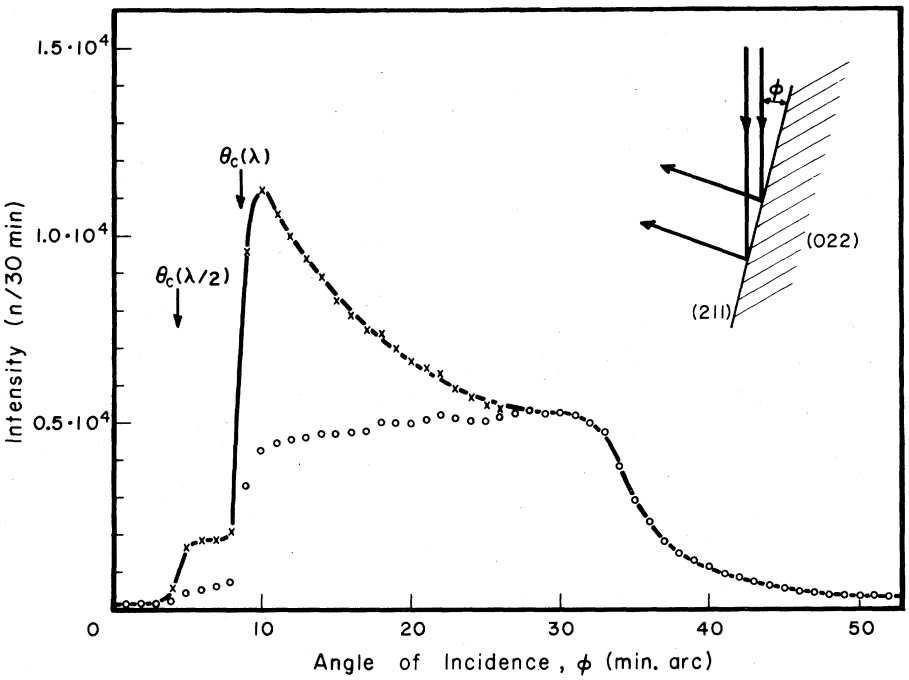

FIG. 15. Experimental result: Bragg diffraction at internal (022) planes in Si of neutrons incident at grazing angles with respect to the (211) surface. The experimentally obtained intensities (○) had to be multiplied by an experimentally determined correction factor to allow for the finite width of the detector slit openings. The result also exhibits some diffracted second-order ($\lambda/2$) intensity.

saic crystal used in the present study. We are currently planning to do experiments of this kind.

The experimental and theoretical results of the present work should also be of interest for future diffraction studies of surfaces. The reduction of the penetration depth for radiation Bragg diffracted in the vicinity of the critical angle may prove useful for studying structures at depths within fractions of micrometers from a surface. For experiments of that kind our observation of a peak in the diffracted intensity just above the critical angle should help to overcome some of the intensity problems expected from the restricting requirement of a good angular definition of the beam used.

On the other hand, in agreement with the experiment, the property that only a very small Bragg reflectivity is predicted for radiation incident at angles just below the critical angle should be applicable to experimentally separate diffraction by the bulk of a specimen from diffraction by a surface layer. To discuss that case we assume the index of refraction of the surface layer to be larger than that of the refractive index of the bulk which is taken to be smaller than unity. In such a case we could conceive of a situation where radiation is incident at an angle just below the critical angle of the bulk material, thus observing only diffraction from the surface layer. A particular example where an arrangement of this type may prove to be useful could be the diffraction from the surfaces of ferromagnets[10] in order to analyze the behavior of the magnetization close to a surface boundary. Here the appropriate conditions for the critical angles could be met by the use of polarized neutrons.

It is evident that similar considerations would also apply to the case of x-ray diffraction. Furthermore, we note that in many of these surface diffraction cases we expect the diffraction problem to be that of diffraction from a two-dimensional lattice due to the small thickness of the surface layer. A similar behavior was predicted by Vineyard[10] for diffraction *below* the critical angle and it will be interesting to compare in detail his approach with the one presented in this paper.

ACKNOWLEDGMENTS

We wish to thank Professor C. G. Shull for stimulating encouragement and critical comments provided during the course of the present work. We acknowledge useful discussions with Mr. John Arthur and Professor M. A. Horne as well as the expert fabrication by Mr. A. Daddario of the devices used in the experiment. Mr. E. J. Alexander gave useful advice on the preparation of the mirror crystal surface and Ms. J. Tobin provided help during some phases of the experiment. This work was supported by the U.S. Department of Energy, Contract No. DE-AC02-76ER03342.A007.

[1]R. W. James, *The Optical Principles of the Diffraction of X-Rays* (Bell, London, 1948).
[2]B. W. Batterman and H. Cole, Rev. Mod. Phys. 36, 681 (1964).
[3]H. Rauch and D. Petrascheck, in *Neutron Diffraction*, edited by H. Dachs (Springer, Berlin, 1978).
[4]P. Farwig and H. W. Schürmann, Z. Phys. 204, 489 (1967).
[5]S. Kishino and K. Kohra, Jpn. J. Appl. Phys. 10, 551 (1971).
[6]O. Brümmer, H. R. Höche, and J. Nieber, Phys. Status Solidi A 33, 587 (1976).
[7]J. Härtwig, Exp. Tech. Phys. 26, 535 (1978).
[8]T. Bedynska, Phys. Status Solidi A 19, 365 (1973).
[9]F. Rusticchelli, Philos. Mag. 31, 1 (1975).
[10]G. Vineyard, Phys. Rev. B 26, 4146 (1982).
[11]P. Eisenberger and W. C. Marra, Phys. Rev. Lett. 46, 1081 (1981).